Assessing mucociliary transport of single particles in vivo shows variable speed and preference for the ventral trachea in newborn pigs

Mark J. Hoegger[a], Maged Awadalla[b], Eman Namati[b], Omar A. Itani[b], Anthony J. Fischer[c], Alexander J. Tucker[b], Ryan J. Adam[b], Geoffrey McLennan[b], Eric A. Hoffman[d], David A. Stoltz[a,e,1], and Michael J. Welsh[a,b,f,1]

Departments of [a]Molecular Physiology and Biophysics, [b]Internal Medicine, [c]Pediatrics, [d]Radiology, and [e]Biomedical Engineering, and [f]Howard Hughes Medical Institute, Roy J. and Lucille A. Carver College of Medicine, University of Iowa, Iowa City, IA 52242

Contributed by Michael J. Welsh, December 27, 2013 (sent for review November 20, 2013)

Mucociliary transport (MCT) is an innate defense mechanism that removes particulates, noxious material, and microorganisms from the lung. Several airway diseases exhibit abnormal MCT, including asthma, chronic bronchitis, and cystic fibrosis. However, it remains uncertain whether MCT abnormalities contribute to the genesis of disease or whether they are secondary manifestations that may fuel disease progression. Limitations of current MCT assays and of current animal models of human disease have hindered progress in addressing these questions. Therefore, we developed an in vivo assay of MCT, and here we describe its use in newborn wild-type pigs. We studied pigs because they share many physiological, biochemical, and anatomical features with humans and can model several human diseases. We used X-ray multidetector-row–computed tomography to track movement of individual particles in the large airways of newborn pigs. Multidetector-row–computed tomography imaging provided high spatial and temporal resolution and registration of particle position to airway anatomy. We discovered that cilia orientation directs particles to the ventral tracheal surface. We also observed substantial heterogeneity in the rate of individual particle movement, and we speculate that variations in mucus properties may be responsible. The increased granularity of MCT data provided by this assay may provide an opportunity to better understand host defense mechanisms and the pathogenesis of airway disease.

Mucociliary transport (MCT) depends on the coordinated beating of cilia to propel mucus out of the lung (1–4). In large mammalian lungs, multiple cell types participate in MCT; goblet cells and submucosal glands secrete mucus, airway epithelia and submucosal glands control the quantity and composition of the airway surface liquid, and ciliated epithelial cells propel mucus through ciliary beating. The importance of MCT as a defense mechanism is demonstrated in people with primary ciliary dyskinesia; their cilia are uncoordinated or lack an effective stroke (5–7). As a result, MCT is disrupted, and progressive airway infections and bronchiectasis ensue. Defective MCT is also thought to contribute to other airway diseases, including cystic fibrosis (8–11), asthma (1, 12), and chronic bronchitis (1, 13). Although MCT can be defective in these diseases, it remains uncertain whether MCT is abnormal from the outset and contributes to disease initiation or whether MCT becomes abnormal after the onset of disease and then accelerates injury. Understanding the contribution of abnormal MCT to the origins of airway disease has been hindered by both the limitations of current MCT assays and current animal models of disease.

In vivo assays of MCT have the advantage that transport is examined with physiological populations of airway cell types including submucosal glands and with natural airway humidification. Currently, the most commonly used in vivo MCT assay involves inhalation of aerosols containing radiolabeled particles, and then retention of radioactivity in the lung is recorded over time (14). This procedure has aided understanding of airway disease and is being used to assess therapeutic interventions in humans (15, 16). Although there are attempts to improve the assay, current methods have limitations. For example, spatial resolution is limited to descriptions of central vs. peripheral lung regions with little detailed anatomical information, temporal resolution is limited, only a fraction of the radioaerosol is cleared from the lung during the study, and cough-induced clearance can confound assays. As a result, detection of abnormalities in disease can be difficult. MCT has also been assessed by placing Teflon disks on the tracheal surface and visually assaying their movement through a bronchoscope (17–20) or through chest X-ray (21). The limitations of these in vivo assays have hindered the ability to investigate lung disease at its onset.

In vitro and ex vivo assays of MCT offer advantages in the ability to control the basolateral solution and perform pharmacological manipulations (22–24). In cultured airway epithelia, the lack of submucosal glands, the constraint that liquid and mucus cannot enter or leave the culture, meniscus effects caused by the structures holding cultured epithelia, artificial control of humidity, and the requirement that investigators must add liquid to cultures to assess ciliary movement of material are limitations (22). For ex vivo preparations, washing of the apical surface and artificial humidification can pose challenges.

In this study we investigated MCT in pigs, which offer advantages over mice for assessing MCT in health and disease. For example, the cell types and anatomy of porcine airways are much closer to those of humans than are murine airways (25–30).

PHYSIOLOGY

Significance

Mucociliary transport (MCT) defends lungs by removing particulates, and defective MCT is hypothesized to contribute to the onset of lung diseases such as asthma, chronic bronchitis, and cystic fibrosis. However, testing those hypotheses has been limited by current MCT assays and mouse models of human disease. We developed an in vivo MCT assay in newborn pigs, which share physiological and anatomical features with humans. The X-ray–computed tomographic-based method provided high spatial and temporal resolution. We discovered that particles preferentially travel up the ventral airway surface. We also discovered substantial heterogeneity in rates of individual particle movement, indicating that MCT does not likely involve homogeneous mucus blankets. The granularity of the data may aid understanding of MCT and disease pathogenesis.

Author contributions: M.J.H., M.A., E.N., O.A.I., D.A.S., and M.J.W. designed research; M.J.H., M.A., E.N., O.A.I., A.J.F., A.J.T., and R.J.A. performed research; G.M. and E.A.H. contributed new reagents/analytic tools; M.J.H., M.A., A.J.F., A.J.T., D.A.S., and M.J.W. analyzed data; and M.J.H., D.A.S., and M.J.W. wrote the paper.

The authors declare no conflict of interest.

[1]To whom correspondence may be addressed. E-mail: michael-welsh@uiowa.edu or david-stoltz@uiowa.edu.

This article contains supporting information online at www.pnas.org/lookup/suppl/doi:10.1073/pnas.1323633111/-/DCSupplemental.

Ciliated cells predominate in human airways, whereas Clara cells comprise ~60% of mouse airway epithelial cells (25, 31). Newborn mouse airways have few ciliated cells and no discernable MCT (32). Mouse intralobular airways lack mucus and serous cells found in humans (31). The pattern of maturation and development of submucosal glands in pigs are comparable with humans (25, 27, 28, 33). Pigs have submucosal glands in the trachea and bronchi, whereas mice have only a few submucosal glands near the larynx and upper trachea (34, 35). In addition, the size of pigs is closer to that of humans than mice, the general anatomic distribution of porcine airways recapitulates that of humans (25), and porcine and human submucosal glands appear to use the same pathways to control and regulate secretion (36, 37). Pigs can also provide models of airway diseases such as cystic fibrosis (38–43).

Our goal was to develop an in vivo assay of MCT that met several criteria: adapts to study of newborn pigs, has the spatial resolution to measure individual particles, obtains data in three dimensions, achieves good temporal resolution, registers MCT to airway anatomy, and uses natural airway humidification.

Results

High-Resolution Chest MDCT Tracks Individual Tantalum Particles in Vivo. To measure MCT we developed a multidetector-row–computed tomographic (MDCT)-based assay. In sedated newborn pigs, we placed a catheter just through the vocal cords, insufflated radiopaque disks into the airways with a puff of air, and immediately removed the catheter (Fig. S1*A*). We used 350 × 25-μm tantalum disks because they are radiodense and chemically inert. Piglets were supine and breathed spontaneously through the nose. Three to sixteen particles were present in the airways at a position beneath the opening to the right cranial lobe, which we used as an anatomical landmark. We acquired volumetric MDCT scans of the apical–basal extent of the lung every 15 s for 10 min for a total of 40 scans (Fig. S1*B*). We then identified individual particles in three dimensions (Fig. 1 *A*–*C*).

We reconstructed the airway anatomy and particle positions; Fig. 2*A* and Movie S1 show ventral–dorsal images from one animal. Symbols and lines of a single color represent the path of individual particles. Symbols indicate a particle's position at 15-s intervals, and lines connect the dots. Particles either moved toward the larynx or were stationary; they never moved distally. A lateral view of the same airway reconstruction suggested that particles preferentially traveled to the ventral surface of the trachea (Fig. 2*B* and Movie S2).

Speed of Individual Particle Movement Shows Substantial Heterogeneity. Individual particles traveled at an average speed of 6.9 ± 0.7 mm/min (mean ± SEM, 57 particles in seven pigs). This rate is similar to that previously reported in excised porcine trachea [2.3 mm/min by particle transport (24) and 5.4 mm/min by optical coherence tomography (44)]. However, the average speed masks substantial heterogeneity. Fig. 3*A* shows the mean speed for individual particles. In one animal (red circles) the mean speed of the fastest moving particle was ~4 times faster than the mean speed of the slowest-moving particle. The maximum speed of individual particles showed the same variation (Fig. 3*B*), and data for all of the animals showed variation in maximal and mean particle speed.

All particle movement had a component directed toward the larynx, but at times, some particles were immobile. In six of seven animals all of the particles exhibited some movement. However, in one pig, half of the particles advanced toward the larynx, and half exhibited no movement. Most particles remained in motion during the entire tracking period, but a few particles were stationary during some portion of the tracking period (Fig. 4*A*). For those particles that were stationary for at least 1 min, that period of immobility occurred at the start of the tracking period in 52% of the cases. Fig. 4*B* shows an example of six particles in one animal. Two of the particles (#4 and #6) were stationary for more than 3 min and then began to move. Moreover, the speed of individual disks changed during the scanning time. Often the rate of movement increased during the course of the run (Fig. 4*B*). For example, the speed during the first minute of tracking was slower than during the third minute for 33% of particles (n = 43 particles). However, we also observed that particles occasionally slowed and/or temporarily stopped during the course of a run (Fig. 4*B*).

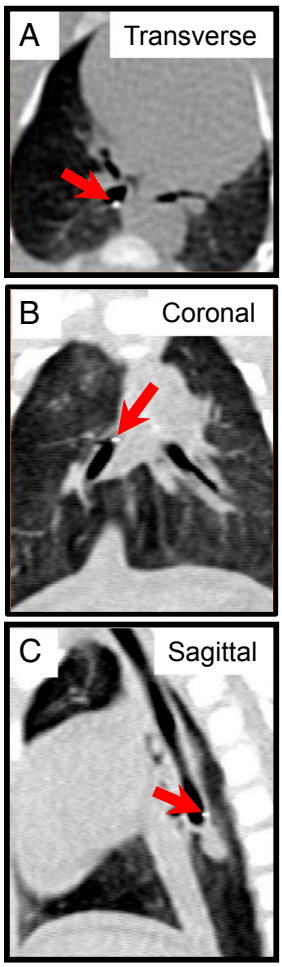

Fig. 1. MDCT scans track particles in airways of newborn pigs. Tantalum disks are more radiodense than surrounding tissue and appeared as bright white dots (red arrows) in transverse (*A*), coronal (*B*), and saggital (*C*) sections of MDCT scans. Disks appear larger than they are because of spillover effects.

Particles Preferentially Travel to the Ventral Trachea. To assess particle position around the circumference of the airways, we established a polar coordinate system in which the airway lumen viewed through a transverse section is treated as a circle, the most ventral point is 0 degrees, and the most dorsal point of the circle is 180 degrees (Fig. 5*A* and Movie S3). We plotted position on the airway circumference of particles in the first scan and in the last scan before they exited the field toward the larynx or at the end of the 10-min scanning period (Fig. 5*B*). In the first scan, particles were distributed evenly throughout the airway circumference. However, by the last scan, they were grouped toward the ventral part of the airway. Angular position had little influence on the speed of particles (Fig. 6).

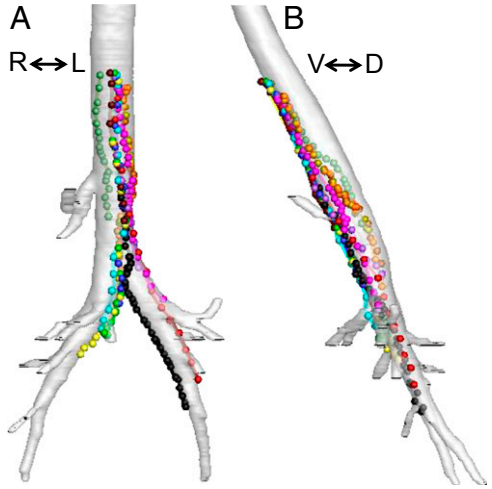

Fig. 2. Individual particles travel up the airways of newborn pigs. Images are reconstructed ventral–dorsal (*A*) and lateral (*B*) views of airways. Individual particles are represented as different colored spheres; area of spheres is ~25 times larger than actual particles. Lines connecting spheres indicate path of particles traveling up the airway.

For these studies, animals were supine, and thus the ventral-directed movement was in the opposite direction of gravity. To further test the effect of gravity, we studied two animals in the prone position. The ventral preference persisted in that position (Fig. 5*C*). Thus, particles demonstrated a strong gravity-independent ventral preference in their movement.

Orientation of Cilia Beating Directs Particles to the Ventral Airway Surface. We hypothesized that the direction of cilia beating was responsible for the ventral particle transport. To test this, we removed segments of trachea, opened them with longitudinal cuts either ventrally or dorsally, mounted them flat under Krebs HCO^-_3/CO_2 buffered saline, and used reflected light video microscopy to determine the direction of cilia beating. We plotted the angle between the rostral–caudal axis and the direction vector of ciliary beat (Fig. 7*A*). At the ventral tracheal surface, cilia were oriented parallel to the rostral–caudal axis (Fig. 7*B*). However, as we measured ciliary orientation at positions away from the ventral surface, a component of beat directionality was directed toward the ventral trachea. We observed similar directionality irrespective of whether the trachea was opened ventrally or dorsally.

We also found that cilia beat frequency was relatively similar around the tracheal circumference (Fig. 7*C*), consistent with the observation that the speed of particle movement was little affected by position on the tracheal circumference. Thus, the orientation of cilia beating directs particles toward the ventral surface and the larynx.

Discussion

In this study, we developed a MDCT-based assay to measure MCT in vivo in newborn pigs. The ability to track individual particles in 3D with high spatial and temporal resolution allowed us to discover substantial heterogeneity in MCT, with variation in the speed of particle movement between animals, between individual particles in an animal, and in the movement of single particles at different times. The methodology also revealed that particles travel preferentially to the ventral surface of the trachea.

Movement of Individual Particles Was Highly Variable. The ability to track discrete particles in the lung revealed heterogeneity in MCT speed between individual particles and during the transit of single particles. There are several factors that might contribute to heterogeneity. First, variation in cilia beat frequency could affect MCT speed. However, that seems unlikely because we found that beat frequency was relatively similar across multiple regions of the trachea. Second, variable depth of periciliary liquid might be responsible. In earlier work, we showed substantial variability in the depth of periciliary liquid in newborn pigs (45). Because we observed that individual particles moved over the same area of trachea at different speeds, either periciliary liquid depth is not an important factor responsible for heterogeneity in MCT, or periciliary liquid depth varies in a highly dynamic and unrecognized manner. Third, variations in the properties or quantity of mucus or association of discs with mucus might cause heterogeneity in MCT speed. For example, there are reports of substantial variability in rates of secretion from individual submucosal glands (46), viscosity of submucosal gland secretions (47), and tracheal mucus thickness (45, 48). We also speculate that local variations in mucus properties or abundance might explain the observation that particles sometimes slow as they journey toward the larynx. Perhaps disks reach an area where mucus being secreted from a submucosal gland has not yet detached from its origin and thus slows progress of the particle. This variability suggests that the trachea, at least in the newborn, is not likely covered by a continuous, homogeneous blanket of mucus (49). If that were the case, we would have expected a more uniform rate of movement. Instead, mucus might function as islands or discrete units, and the rates of movement may vary even in similar airway regions.

Ciliary Orientation Preferentially Moves Particles to the Ventral Tracheal Surface for Removal from the Lung in Newborn Pigs. We discovered that particles traveled to the ventral tracheal surface as they progressed toward the larynx. This ventral-directed flow pattern is reminiscent of the flow of cars from an on-ramp onto an interstate highway. That is, the ventral tracheal wall is analogous to the highway, and the dorsal and lateral walls are analogous to on-ramps. However, in contrast to a highway system, particle speed was independent of position.

The direction of ciliary beating must have been established in the fetus because it was present immediately after birth. Thus, it cannot be attributed to gravity during development, and it was not gravity-dependent during testing. Although a core set of planar cell polarity proteins are known to establish the orientation of cilia

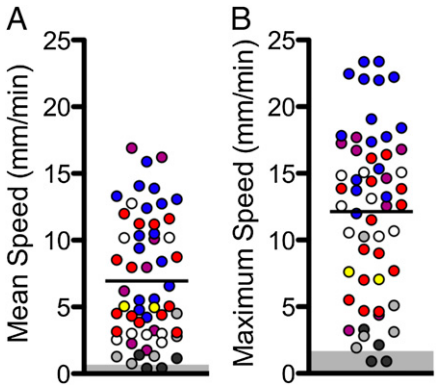

Fig. 3. Rate of particle movement is heterogeneous. Data are speeds of tantalum particles in newborn pigs. Each symbol indicates a different animal, and multiple points of the same symbol represent individual particles from the same animal. $n = 7$ pigs. Each point represents an individual particle's mean speed (*A*) and maximum speed (*B*). Bar indicates mean. The mean and maximum disk speeds were not corrected for animal movement. We measured the range of speeds for movement of the anatomical landmarks, and they are shown by the gray boxes in *A* and *B*.

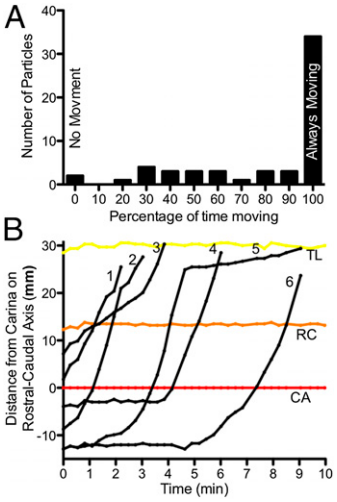

Fig. 4. Speed of individual particles varies with time. (*A*) Histogram showing the percentage of time that particles moved during a scanning period or until they traveled above the apex of the lung. For example, two particles did not move during the 10-min scanning period. (*B*) Example showing position of six particles (numbered 1–6, black) in relation to the rostral–caudal axis. Anatomical landmarks are the lung apex (TL), the right cranial lobe bronchus (RC), and the carina (CA). Distances distal to the carina are given as negative values.

in the airways, the global directional cues remain uncertain (50). Perhaps the pattern of cilia orientation in the pigs could facilitate discovery of the responsible signals.

The ventral preference for MCT in pigs contrasts with earlier studies in dogs; bronchoscopic observations suggested that when viewed from above, particles moved in a clockwise (or counterclockwise in a few dogs) orientation around the trachea, and some accumulated on the dorsal surface where they traveled cephalad (18, 19, 51). In the pig, submucosal glands are most abundant in the dorsal wall, followed by the ventral and then lateral walls (52). This distribution and frequency are relatively unique among experimental laboratory animals in that the preferential dorsal vs. ventral distribution is similar to that in humans (53). We speculate that dorsally secreted mucus sweeps around the trachea to maximally capture particulates and then concentrates in a smaller area ventrally. Gathering mucus in this way rather than having it spread evenly around the tracheal circumference might make it more susceptible to the shear force of air generated by coughing and hence facilitate its expulsion from the lung. In the dog, ventrally secreted mucus might have the reverse pattern.

This Method for Measuring MCT Has Advantages and Limitations. Our approach has several advantages. In this in vivo approach, piglets breathed spontaneously through their noses so normal airway humidification was maintained. By using volumetric MDCT scans and recording the position of discrete particles at 15-s intervals, we were able to obtain high spatial and temporal resolution. The use of MDCT scans also allowed us to register the position of particles to the airway anatomy. As with other imaging methods, increasing the granularity of the data revealed interesting patterns of MCT.

This method also has a number of limitations. (*i*) The amount of radiation exposure used in this study is greater than with radiolabeled aerosols and thus not acceptable for human use. (*ii*) The animals were sedated. We used ketamine and acepromazine for initial sedation and then propofol to maintain sedation. Previous studies indicate that these agents are not likely to alter MCT, ciliary beat frequency, or mucus secretion (54–56). (*iii*) The size of the tantalum particles (350 × 25 μm) is larger than bacteria and some particulates that enter the lung. However, studies using other methods and larger and smaller particles suggest that MCT is not markedly altered by particle size, although small particles might be ingested by macrophages (51, 57, 58). Moreover, earlier studies reported transport rates that encompass the range of MCT we measured (59, 60). (*iv*) The method does not assess small airways; we currently have only deposited particles from the trachea to third generation airways. However, studying more distal airways could be of value. Although most airway diseases involve both small and large airways after the disease is established, much less is known about the distribution of abnormalities at the onset of disease. (*v*) The number of particles deposited in an airway is small and could therefore miss additional complexity. However, we used a small number to adequately discriminate individual particles as they advanced up the airway.

Concluding Comments. We anticipate that this method may be adapted for several applications. Because of its sensitivity, it may be of value in revealing differences between wild-type animals and those with disease, including cystic fibrosis, asthma, and chronic bronchitis. These methods may be especially helpful early in the course of disease, and the ability to assess heterogeneity may provide insight into pathophysiological mechanisms. It may also be of use for assessing the response to interventions that may alter the function of individual components of the MCT process, including cilia, mucus-producing goblet cells and submucosal glands, and transepithelial electrolyte transport by airway epithelia. Finally, probing MCT at greater resolution in pigs may help guide efforts to improve MCT assays for humans.

Materials and Methods

Animals. Newborn wild-type domestic pigs were used for these studies. Pigs were euthanized with IV euthasol (Virbac) injection followed by bilateral

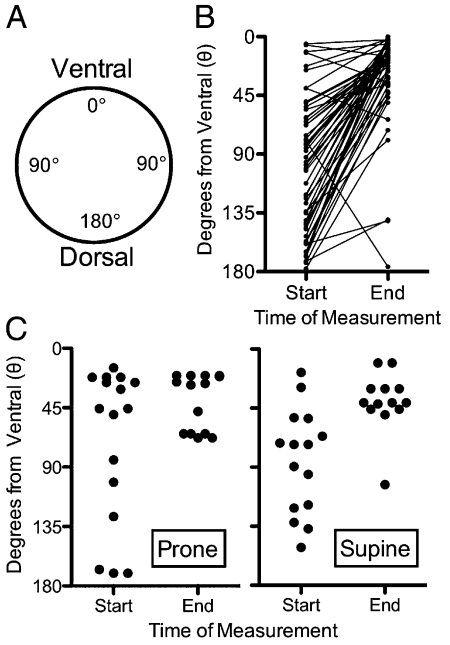

Fig. 5. Particles are transported to the ventral trachea surface independent of animal position. (*A*) Schematic showing position on the airway in degrees. Degree coordinates are given as absolute values with no designation for left or right. (*B*) Radial positions at start and end of the 10-min scanning period. Particles moved to a more ventral position during the scanning period ($n = 7$ pigs, 55 particles, $P \leq 0.0001$, paired Student t test). (*C*) Radial positions at start and end of 10-min scanning periods for two piglets studied in the prone and then supine positions. Individual particles were not tracked, and some had left the scanning region in the final scan.

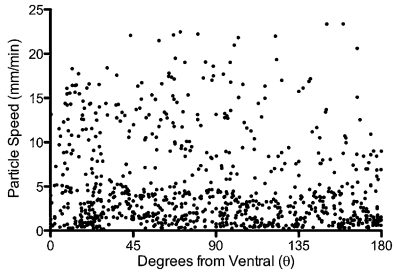

Fig. 6. Angular position had little influence on particle speed. Data are polar coordinate position on the *x* axis and particle speed on the *y* axis. n = 55 particles in 7 animals.

thoracotomy. All animal protocols were approved by the University of Iowa Institutional Animal Care and Use Committee.

In Vivo Mucociliary Transport Assay. Tantalum disks (350 × 25-μm) were punched from tantalum foil (Sigma). The average particle mass was 55 μg. Newborn pigs were anesthetized with 20 mg/kg ketamine and 2 mg/kg acepromazine delivered IV, and then sedation was maintained with IV propofol. Pigs breathed spontaneously through the nose. To deliver tantalum particles, animals were briefly intubated, and 15–30 tantalum disks were insufflated into the lungs with a puff of air (Fig. S1*A*). Immediately after particle delivery, the catheter was removed. To assess particle transport, serial three-dimensional images of the chest were acquired with a high-resolution multirow detector computerized tomography scanner (Siemens Somatom, Definition Flash Dual Source 128-slice computed tomography (CT) Scanner; Fig. S1*B*). MDCT-generated Digital Imaging and Communications in Medicine (DICOM) images were taken with a slice depth of 0.6 mm and a slice interval of 0.3 to ensure visualization of tantalum particles. Unless specified, scans were performed with the pig in the supine position. Over a 10-min acquisition period, a total of 40 scans were taken with a 15-s interval between scans. The tantalum particles, with typical Hounsfield units of 500, were easily discerned from surrounding airway tissue, which had Hounsfield units of approximately −200 (Fig. 1 *A*–*C*). Individual particles were manually tracked by assigning three-dimensional Cartesian coordinates with a time value depending on the scan (*x*, *y*, *z*, time) using ImageJ for DICOM image analysis. To avoid alterations in the airway surface due to the presence of the delivery catheter, particles were not tracked once they traveled above the position of the lung apex. Only particles that were delivered beyond the right cranial lobe were tracked to provide enough distance to appropriately analyze transport. To determine particle speed, we measured the distance particles moved over a known period. Movement from spontaneous breathing could confound measures of transport rate. To avoid this, we determined the average position of three anatomical landmarks in each pig: the right cranial lobe opening (RC), the carina (CA), and the lung apex (AP). We discarded any scan in which the position of the three landmarks deviated more than 1 mm from the average position of the landmarks. We then used the subsequent scan to calculate speed. This correction removed 2.5% of the scans.

Calculation of speed using 15-s intervals exaggerates the contribution of any animal movement to speed. Therefore, to reduce noise in calculating speed, we measured particle position every 15 s and used 60-s intervals to calculate speed. These approaches generated multiple measurements of speed for each particle. We used the following equation to calculate particle speed.

$$\text{Particle Speed} = \text{SQRT}\left((X_{n+4}-X_n)^2+(Y_{n+4}-Y_n)^2+(Z_{n+4}-Z_n)^2\right)\Big/(t_{n+4}-t_n)$$

where n refers to the number of the scan, *x*, *y*, *z* represent Cartesian coordinates (*x*, left–right; *y*, dorsal–ventral; *z*, rostral–caudal), and *t* represents time in minutes.

In some examples, we show speed as the maximum particle speed, which is the highest value for speed generated by an individual particle. In other cases, we show the mean speed, which is the average of all speed values generated by an individual particle. Multiple measurements of particle speed for an individual animal allows us to display more speed values than there are total particles; this is seen in the speed vs. angular position assessment. Only particles that traveled more than 3 mm were included in speed vs. angular position assessments.

To assess how many of the particles delivered to an airway were immobile, we determined how many particles moved less than 3 mm over the course of the 10-min scanning interval. Three millimeters is a conservative estimate that negates the possibility that an artifact from animal movement will lead to an incorrect scoring of an immobile particle.

To quantify the position of a particle relative to the ventral–dorsal axis, we developed a radial coordinate system. Using transverse MDCT sections, the airway was treated as a circle where the most ventral portion of the airway was designated a radial coordinate of 0 degrees, and the most dorsal aspect was designated 180 degrees. To determine the radial coordinate of particles in relation to the trachea, two-dimensional Cartesian coordinates were acquired at the following points: the position of the center of the airway lumen (X_c,Y_c), the position of the most ventral airway (X_a,Y_a), and the position of the particle on the airway surface (X_p,Y_p). From these points, we determined the radial position of the particle using the following equation derived from the law of cosines:

$$\text{Radial Coordinate Position} = \text{Arccos}\left((a^2+b^2-c^2)/(2ab)\right)$$
$$a = \text{Sqrt}\left((X_c-X_a)^2+(Y_c-Y_a)^2\right)$$
$$b = \text{Sqrt}\left((X_c-X_p)^2+(Y_c-Y_p)^2\right)$$
$$c = \text{Sqrt}\left((X_a-X_p)^2+(Y_a-Y_p)^2\right)$$

The absolute value of the radial coordinate is represented with no designation for the right or left side of the airway. For one set of experiments, we examined the radial coordinates of disks at time 0 and 10 min with the pig in the prone and supine positions. During the experiments, some particles likely left the tracking area and were not included in the 10-min time points.

Ex Vivo Cilia Orientation and Beat Frequency Analysis. To asses cilia orientation ex vivo, animals were euthanized, and 1-cm–long rings of trachea immediately proximal to the right cranial lobe bronchus were excised and placed in Krebs Ringers solution containing (in mM) 115 NaCl, 25 $NaHCO_3$ 10 glucose, 2.4 K_2HPO_4, 1.2 $CaCl_2$, 1.2 $MgCl_2$, 0.6 KH_2PO_4, pH =7.3 in 5% (vol/vol) CO_2 on ice for 1–4 h. For studies, a longitudinal incision spanning the length of the tracheal ring was made on either the most ventral or dorsal aspect of the ring to make a rectangular sheet. Tracheal sheets were mounted flat by pinning to dental wax, rinsed, and then submerged in 37 °C Krebs Ringers solution pH = 7.3/5% CO_2. We used reflected light to visualize cilia motion (Nikon A1R Resonant Scanning Confocal Microscope, 25× objective [charge-coupled device (CCD) camera and Nikon Imaging System (NIS) elements software, 200 frames/s]. We analyzed 1-s video clips (NIS Elements) to determine cilia orientation and beat

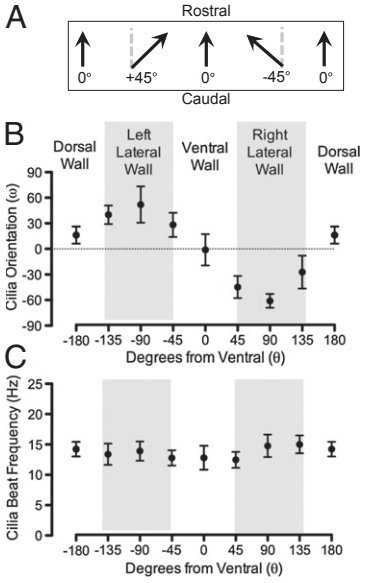

Fig. 7. Cilia orientation determines ventral directed particle movement. Cilia orientation and beat frequency were determined ex vivo using reflected light video microscopy on flat mounts of trachea. (*A*) Schematic shows orientation of cilia. (*B*) Data are cilia orientation (ω) at indicated positions on tracheal circumference. Data are from one animal. n = 7–16 cells per data point; mean ± SD. Similar results were obtained in three other animals. (*C*) Data are cilia beat frequency at indicated positions on tracheal circumference. Data are from one animal. n = 15–30 cells per data point; mean ± SD. Similar results were obtained in three other animals.

PHYSIOLOGY

frequency. To quantify the orientation of cilia we determined the angle between the axis of ciliary beat and the rostral–caudal plane (Fig. 7*A*). To quantify cilia beat frequency, we counted the number of reflected light-intensity change cycles in regions of ciliated cells over a known time period.

Statistical Analysis. Assessment of ventral preference was performed by paired *t* test with the assumption that dorsal–ventral movement was independent of individual piglets.

ACKNOWLEDGMENTS. We thank Elizabeth Allard, Lucas Askland, Suifang Mao, Theresa Mayhew, James McMenimen, Andrew Michalski, Sean Mobberly, Thomas O Moninger, Lynda Ostedgaard, Leah Reznikov, Viral Shah, Jered Sieren, and Peter Taft. This work was supported by the National Institutes of Health (NIH) (HL051670, HL091842, DK054759), the Cystic Fibrosis Foundation, and the Cystic Fibrosis Foundation Mucociliary Clearance Consortium. D.A.S. is supported by the Gilead Sciences Research Scholars Program in Cystic Fibrosis and the NIH (DP2 HL117744). M.J.W. is an Investigator of the Howard Hughes Medical Institute.

1. Fahy JV, Dickey BF (2010) Airway mucus function and dysfunction. *N Engl J Med* 363(23):2233–2247.
2. Chilvers MA, O'Callaghan C (2000) Local mucociliary defence mechanisms. *Paediatr Respir Rev* 1(1):27–34.
3. Smith DJ, Gaffney EA, Blake JR (2008) Modelling mucociliary clearance. *Respir Physiol Neurobiol* 163(1–3):178–188.
4. Voynow JA, Rubin BK (2009) Mucins, mucus, and sputum. *Chest* 135(2):505–512.
5. Sagel SD, Davis SD, Campisi P, Dell SD (2011) Update of respiratory tract disease in children with primary ciliary dyskinesia. *Proc Am Thorac Soc* 8(5):438–443.
6. Leigh MW, et al. (2009) Clinical and genetic aspects of primary ciliary dyskinesia/Kartagener syndrome. *Genet Med* 11(7):473–487.
7. Bush A, et al. (2006) Mucus properties in children with primary ciliary dyskinesia: Comparison with cystic fibrosis. *Chest* 129(1):118–123.
8. Boucher RC (2007) Evidence for airway surface dehydration as the initiating event in CF airway disease. *J Intern Med* 261(1):5–16.
9. Quinton PM (1999) Physiological basis of cystic fibrosis: A historical perspective. *Physiol Rev* 79(1, Suppl):S3–S22.
10. Rowe SM, Miller S, Sorscher EJ (2005) Cystic fibrosis. *N Engl J Med* 352(19):1992–2001.
11. Davis PB (2006) Cystic fibrosis since 1938. *Am J Respir Crit Care Med* 173(5):475–482.
12. Messina MS, O'Riordan TG, Smaldone GC (1991) Changes in mucociliary clearance during acute exacerbations of asthma. *Am Rev Respir Dis* 143(5 Pt 1):993–997.
13. Koblizek V, et al. (2011) Impairment of nasal mucociliary clearance in former smokers with stable chronic obstructive pulmonary disease relates to the presence of a chronic bronchitis phenotype. *Rhinology* 49(4):397–406.
14. Robinson M, Bye PT (2002) Mucociliary clearance in cystic fibrosis. *Pediatr Pulmonol* 33(4):293–306.
15. Bennett WD, Almond MA, Zeman KL, Johnson JG, Donohue JF (2006) Effect of salmeterol on mucociliary and cough clearance in chronic bronchitis. *Pulm Pharmacol Ther* 19(2):96–100.
16. Laube BL, Karmazyn YJ, Orens JB, Mogayzel PJ, Jr. (2007) Albuterol improves impaired mucociliary clearance after lung transplantation. *J Heart Lung Transplant* 26(2):138–144.
17. Wood RE, Wanner A, Hirsch J, Farrell PM (1975) Tracheal mucociliary transport in patients with cystic fibrosis and its stimulation by terbutaline. *Am Rev Respir Dis* 111(6):733–738.
18. Sackner MA, Rosen MJ, Wanner A (1973) Estimation of tracheal mucous velocity by bronchofiberscopy. *J Appl Physiol* 34(4):495–499.
19. Hirsch JA, Swenson EW, Wanner A (1975) Tracheal mucous transport in beagles after long-term exposure to 1 ppm sulfur dioxide. *Arch Environ Health* 30(5):249–253.
20. Gosselink R, Gayan-Ramirez G, Houtmeyers E, de Paepe K, Decramer M (2006) High-dose lidocaine reduces airway mucus transport velocity in intubated anesthetized dogs. *Respir Med* 100(2):258–263.
21. O'Riordan TG, Otero R, Mao Y, Lauredo I, Abraham WM (1997) Elastase contributes to antigen-induced mucociliary dysfunction in ovine airways. *Am J Respir Crit Care Med* 155(5):1522–1528.
22. Matsui H, et al. (1998) Evidence for periciliary liquid layer depletion, not abnormal ion composition, in the pathogenesis of cystic fibrosis airways disease. *Cell* 95(7):1005–1015.
23. Ballard ST, Parker JC, Hamm CR (2006) Restoration of mucociliary transport in the fluid-depleted trachea by surface-active instillates. *Am J Respir Cell Mol Biol* 34(4):500–504.
24. Cooper JL, Quinton PM, Ballard ST (2013) Mucociliary transport in porcine trachea: differential effects of inhibiting chloride and bicarbonate secretion. *Am J Physiol Lung Cell Mol Physiol* 304(3):L184–L190.
25. Rogers CS, et al. (2008) The porcine lung as a potential model for cystic fibrosis. *Am J Physiol Lung Cell Mol Physiol* 295(2):L240–L263.
26. Mariassy AT (1992) Epithelial cells of trachea and bronchi. *Comparative Biology of the Normal Lung*, ed Parent RA (CRC Press, Boca Raton, FL), pp 63–76.
27. Mills AN, Lopez-Vidriero MT, Haworth SG (1986) Development of the airway epithelium and submucosal glands in the pig lung: Changes in epithelial glycoprotein profiles. *Br J Exp Pathol* 67(6):821–829.
28. Baskerville A (1976) Histological and ultrastructural observations on the development of the lung of the fetal pig. *Acta Anat (Basel)* 95(2):218–233.
29. Jones R, Baskerville A, Reid L (1975) Histochemical identification of glycoproteins in pig bronchial epithelium: (a) Normal and (b) hypertrophied from enzootic pneumonia. *J Pathol* 116(1):1–11.
30. Winkler GC, Cheville NF (1984) The neonatal porcine lung: Ultrastructural morphology and postnatal development of the terminal airways and alveolar region. *Anat Rec* 210(2):303–313.
31. Pack RJ, Al-Ugaily LH, Morris G (1981) The cells of the tracheobronchial epithelium of the A quantitative light and electron microscope study. *J Anat* 132(Pt 1):71–84.
32. Francis RJ, et al. (2009) Initiation and maturation of cilia-generated flow in newborn and postnatal mouse airway. *Am J Physiol Lung Cell Mol Physiol* 296(6):L1067–L1075.
33. Sturgess J, Imrie J (1982) Quantitative evaluation of the development of tracheal submucosal glands in infants with cystic fibrosis and control infants. *Am J Pathol* 106(3):303–311.
34. Wine JJ, Joo NS (2004) Submucosal glands and airway defense. *Proc Am Thorac Soc* 1(1):47–53.
35. Plopper CG, et al. (1983) Comparison of nonciliated tracheal epithelial cells in six mammalian species: Ultrastructure and population densities. *Exp Lung Res* 5(4):281–294.
36. Choi JY, et al. (2007) Synergistic airway gland mucus secretion in response to vasoactive intestinal peptide and carbachol is lost in cystic fibrosis. *J Clin Invest* 117(10):3118–3127.
37. Baniak N, Luan X, Grunow A, Machen TE, Ianowski JP (2012) The cytokines interleukin-1β and tumor necrosis factor-α stimulate CFTR-mediated fluid secretion by swine airway submucosal glands. *Am J Physiol Lung Cell Mol Physiol* 303(4):L327–L333.
38. Rogers CS, et al. (2008) Disruption of the CFTR gene produces a model of cystic fibrosis in newborn pigs. *Science* 321(5897):1837–1841.
39. Ostedgaard LS, et al. (2011) The ΔF508 mutation causes CFTR misprocessing and cystic fibrosis-like disease in pigs. *Sci Transl Med* 3(74):74ra24.
40. Stoltz DA, et al. (2010) Cystic fibrosis pigs develop lung disease and exhibit defective bacterial eradication at birth. *Sci Transl Med* 2(29):29ra31.
41. Pezzulo AA, et al. (2012) Reduced airway surface pH impairs bacterial killing in the porcine cystic fibrosis lung. *Nature* 487(7405):109–113.
42. Lee RJ, Foskett JK (2010) cAMP-activated Ca2+ signaling is required for CFTR-mediated serous cell fluid secretion in porcine and human airways. *J Clin Invest* 120(9):3137–3148.
43. Cho HJ, Joo NS, Wine JJ (2011) Defective fluid secretion from submucosal glands of nasal turbinates from CFTR-/- and CFTR (ΔF508/ΔF508) pigs. *PLoS ONE* 6(8):e24424.
44. Liu L, et al. (2013) Method for quantitative study of airway functional microanatomy using micro-optical coherence tomography. *PLoS ONE* 8(1):e54473.
45. Chen J-H, et al. (2010) Loss of anion transport without increased sodium absorption characterizes newborn porcine cystic fibrosis airway epithelia. *Cell* 143(6):911–923.
46. Joo NS, Wu JV, Krouse ME, Saenz Y, Wine JJ (2001) Optical method for quantifying rates of mucus secretion from single submucosal glands. *Am J Physiol Lung Cell Mol Physiol* 281(2):L458–L468.
47. Jayaraman S, Joo NS, Reitz B, Wine JJ, Verkman AS (2001) Submucosal gland secretions in airways from cystic fibrosis patients have normal [Na(+)] and pH but elevated viscosity. *Proc Natl Acad Sci USA* 98(14):8119–8123.
48. Sims DE, Horne MM (1997) Heterogeneity of the composition and thickness of tracheal mucus in rats. *Am J Physiol* 273(5 Pt 1):L1036–L1041.
49. Sears PR, Davis CW, Chua M, Sheehan JK (2011) Mucociliary interactions and mucus dynamics in ciliated human bronchial epithelial cell cultures. *Am J Physiol Lung Cell Mol Physiol* 301(2):L181–L186.
50. Vladar EK, Bayly RD, Sangoram AM, Scott MP, Axelrod JD (2012) Microtubules enable the planar cell polarity of airway cilia. *Curr Biol* 22(23):2203–2212.
51. Asmundsson T, Kilburn KH (1970) Mucociliary clearance rates at various levels in dog lungs. *Am Rev Respir Dis* 102(3):388–397.
52. Meyerholz DK, et al. (2010) Loss of CFTR function produces abnormalities in tracheal development in neonatal pigs and young children. *Am J Respir Crit Care Med* 182(10):1251–1261.
53. Choi HK, Finkbeiner WE, Widdicombe JH (2000) A comparative study of mammalian tracheal mucous glands. *J Anat* 197(Pt 3):361–372.
54. Padda GS, Kishioka C, Rubin BK (2001) Propofol and methohexital have no significant effect on mucus secretion or clearance in the anesthetized dog. *Crit Care Med* 29(5):1045–1048.
55. Hann HC, Hall AP, Raphael JH, Langton JA (1998) An investigation into the effects of midazolam and propofol on human respiratory cilia beat frequency in vitro. *Intensive Care Med* 24(8):791–794.
56. Iida H, Matsuura S, Shirakami G, Tanimoto K, Fukuda K (2006) Differential effects of intravenous anesthetics on ciliary motility in cultured rat tracheal epithelial cells. *Can J Anaesth* 53(3):242–249.
57. Stewart WC (1948) Weight-carrying capacity and excitability of excised ciliated epithelium. *Am J Physiol* 152(1):1–5.
58. Henning A, et al. (2010) Influence of particle size and material properties on mucociliary clearance from the airways. *J Aerosol Med Pulm Drug Deliv* 23(4):233–241.
59. Boothe HW, Boothe DM, Komkov A, Longnecker MT, Hightower D (1993) Tracheal mucociliary transport rate in awake dogs. *Am J Vet Res* 54(11):1812–1816.
60. Tomkiewicz RP, et al. (1995) Species differences in the physical and transport properties of airway secretions. *Can J Physiol Pharmacol* 73(2):165–171.